Journal of
Chemical Engineering & Process Technology

Uchiyama and Kishimoto, J Chem Eng Process Technol 2014, 5:6
DOI: 10.4172/2157-7048.1000207

Research Article Open Access

Numerical Simulation of Air-water Bubbly Jet Issuing from a Square Nozzle by a Vortex in Cell Method

Tomomi Uchiyama[1]* and Yusuke Kishimoto[2]

[1]EcoTopia Science Institute, Nagoya University, Furo-cho, Chikusa-ku, Nagoya 464-8603, Japan
[2]Fujitsu Limited, 1-5-2 Higashi-Shimbashi, Minato-ku, Tokyo 105-7123, Japan

Abstract

A water jet entrained with small air bubbles is simulated. The Vortex in Cell method for bubbly flow proposed by the authors in a prior study is used for the simulation. The method discretizes the vorticity field into vortex elements and computes the time evolution of the flow by tracing the convection of each vortex element using the Lagrangian approach. The bubbly jet issues vertically upward from a nozzle of square cross-section. The Reynolds number based on the water velocity is 5000. The bubble diameter is 0.2 mm, and the bubble volumetric flow rate ratio at the nozzle is 0.0025. The bubbles increase the water turbulence intensity around the jet centerline. This makes the water momentum diffusion in the lateral direction larger at the initial region of the jet. The bubble effect lessens with increasing axial distance from the nozzle. These simulated results are favorably compared with existing measurements, demonstrating the validity of the current simulation method for bubbly jet. In the developed region, the water velocity decay is relaxed and the half-width reduces. This is because the water is accelerated by the bubbles, which have higher axial velocity due to the buoyant force.

Keywords: Gas-liquid bubbly flow; CFD; Jet; Vortex in cell method; Bubble behavior

Notations: B: side length of nozzle cross-section [m]; b: half-width for single-phase water jet [m]; d: bubble diameter [m]; Eo: Eötvös number $=g(\rho_l-\rho_g)d^2/\sigma$ [-]; g: gravitational constant [m/s^2]; p: pressure [Pa]; Q: second invariant of the water velocity gradient tensor [1/s^2]; Re: Reynolds number$=U_0B/\nu_l$ [-]; Re$_b$: bubble Reynolds number$=d|\boldsymbol{u}_g-\boldsymbol{u}_l|/\nu_l$ [-]; t: time [s]; u: velocity [m/s]; U_0: water velocity at nozzle exit [m/s]; v: volume of single bubble$=\pi d^3/6$ [m^3]; W: redistribution function of vorticity [-]; x, y, z: orthogonal coordinates [m]; α: volume fraction [-]; β: density ratio$=\rho_g/\rho_l$ [-]; Δt: time increment [s]; Δx, Δy, Δz: grid width in direction of x, y, z [m]; ν: kinematic viscosity [m^2/s]; ρ: density [kg/m^3]; σ: surface tension [kg/s^2]; ϕ: scalar potential [m^2/s]; ψ: vector potential [m^2/s]; ω: vorticity of liquid-phase$=\nabla\times\boldsymbol{u}_l$ [1/s]; c: jet centerline; g: gas-phase; l: liquid-phase; rms: root mean square; x, y, z: components in directions of x, y, z

Introduction

Vortex in Cell (VIC) method is one of the vortex methods simulating incompressible flows [1]. It discretizes the vorticity field into vortex elements and computes the time evolution of the flow by tracing the convection of each vortex element using the Lagrangian approach. The Lagrangian calculation markedly reduces numerical diffusion and also improves numerical stability. Thus, the VIC method is eminently suitable for direct numerical simulation (DNS) of turbulent flows. Cottet and Poncet [2] applied the VIC method to the wake simulation of a circular cylinder mounted in a uniform flow field and successfully captured the stream wise vortices occurring behind the cylinder. Cocle et al. [3] analyzed the behavior of two vortex system near a solid wall and made clear the interaction between the two counter-rotating vortices and the eddies induced in the vicinity of the wall. Chatelain et al. [4] simulated the interaction between trailing vortices and visualized the unsteady phenomena caused by disturbances. These studies demonstrate the applicability of the DNS by the VIC method to free turbulent flows which are dominated by the convection of large-scale eddies.

The authors [5] have previously proposed two improvements of the VIC method. First, a staggered-grid discretization method guarantees consistency among the discretized equations and prevents numerical oscillations in the solution. Second, a correction method for the vorticity enables the computation of vorticity fields satisfying the solenoidal condition. The improved VIC method was applied to the DNS of a turbulent channel flow [5]. The DNS highlighted the successful capture of organized flow structures, such as streaks and streamwise vortices in the near wall region, demonstrating that the VIC method is applicable to DNS of wall turbulent flows. Uchiyama [6] presented a simulation method for bubbly flow by using the VIC method. The behavior of vortex element and the bubble motion are simultaneously analyzed by the Lagrangian method. Uchiyama [7] also proposed a VIC method for incompressible gas flows laden with small solid particles. This method was favorably validated in simulations of small free-falling solid particles in unbounded air [7]. Uchiyama and Shimada [8] used the VIC method to simulate the interaction between a vortex pair and small solid particles near a horizontal wall in the air. The simulation made clear the agitation of particles by the vortex pair approaching the wall, the production of vorticity fields by the particles, and the particle-induced changes in the strength and behavior of the vortex pair.

Liquid jets entraining small gas bubbles are utilized in equipment, such as chemical reactors, heat exchangers and aerators. A number of experimental researches were conducted to investigate the relationship between the large-scale eddies and the bubble distribution [9] as well

***Corresponding author:** Tomomi Uchiyama, Eco Topia Science Institute, Nagoya University, Furo-cho, Chikusa-ku, Nagoya 464-8603, Japan, Tel: +81-52-789-5187; Fax: +81-52-789-5187; E-mail: uchiyama@is.nagoya-u.ac.jp

Received August 29, 2014; **Accepted** September 26, 2014; **Published** September 30, 2014

Citation: Uchiyama T, Kishimoto Y (2014) Numerical Simulation of Air-water Bubbly Jet Issuing from a Square Nozzle by a Vortex in Cell Method. J Chem Eng Process Technol 5: 207. doi: 10.4172/2157-7048.1000207

as the bubble effect on the liquid velocity field [10-14]. But there are no numerical simulations except for a few studies. Sun and Faeth [10,11] simulated a bubbly jet. But they assumed an axisymmetric flow to employ a k-ε model [15] developed for gas-particle two-phase flow. Thus, the validity of the simulation is unclear. Xing et al. [16] reported a DNS for a cavitating jet. As they applied a homogeneous model which assumes the gas and the liquid have the same velocity, the interactions between the two phases were not fully analyzed. Consequently, a reliable simulation method for bubby jets is not presented.

In this study, the author's VIC method for bubbly flow [6] is applied to simulate an air-water bubbly jet issuing vertically upward from a nozzle into quiescent water. The Reynolds number based on the water velocity is 5000, and the bubbles having a diameter 0.2 mm are issued from the nozzle with the same velocity as the water. The bubble volumetric flow rate ratio at the nozzle is 0.0025. The simulation clarifies the effects of the bubbles on the water flow, such as the changes in the vorticity field and the relaxation of the velocity decay at the jet initial region. It also highlights that such simulated results are in good agreement with the measured ones of Kumar et al. [12], demonstrating the validity and applicability of the VIC method to bubbly jet simulations.

Basic Equations and Numerical Method

Assumptions

The following assumptions are employed for the simulation:

(a) The mixture is a gas-liquid bubbly flow entraining small bubbles.

(b) Both phases are incompressible and no phase changes occur.

(c) The mass and momentum of the gas-phase are very small and negligible compared with those of the liquid-phase.

(d) The bubbles maintain their spherical shape, and neither fragmentation nor coalescence occurs.

Governing equations for bubbly flow

The mass conservation equation for the liquid-phase and that for the gas-phase are independently derived. Taking the summation of them and rearranging the resultant equation with the assumptions (a)-(c), the mass conservation equation for the two-phase mixtures is obtained [6]:

$$\frac{\partial \alpha_l}{\partial} + \nabla \cdot (\alpha_l \boldsymbol{u}_l) = 0 \tag{1}$$

where α_l is the liquid volume fraction satisfying the following relation with the gas volume fraction α_g:

$$\alpha_g + \alpha_l = 1 \tag{2}$$

The momentum conservation equation for the two-phase mixtures, which is also derived from the equations for each phase by the same manner as the mass conservation equation, is expressed as [6]:

$$\alpha_l \frac{D\boldsymbol{u}_l}{Dt} = \frac{1}{\rho_l}\nabla p + \nu_l \nabla^2 \boldsymbol{u}_l + \alpha_l \boldsymbol{g} \tag{3}$$

where $D\boldsymbol{u}_l / Dt = \partial \boldsymbol{u}_l / \partial t + (\boldsymbol{u}_l \cdot \nabla)\boldsymbol{u}_l$.

It is postulated that the virtual mass force, the drag force, the gravitational force, and the lift force act on the bubble. In this case, the equation of motion for the bubble is expressed by the following equation [17,18] with the assumption (d):

$$\frac{\mathrm{d}\boldsymbol{u}_g}{\mathrm{d}t} = \frac{1+C_V}{\beta+C_V}\frac{\mathrm{D}\boldsymbol{u}_l}{\mathrm{D}t} - \frac{1}{\beta+C_V}\frac{3C_D}{4d}|\boldsymbol{u}_g - \boldsymbol{u}_l|(\boldsymbol{u}_g - \boldsymbol{u}_l) + \frac{\beta-1}{\beta+C_V}\boldsymbol{g} - \frac{C_L}{\beta+C_V}(\boldsymbol{u}_g - \boldsymbol{u}_l)\times(\nabla\times\boldsymbol{u}_l) \tag{4}$$

where d is the bubble diameter, and β is the density ratio defined as $\rho_g/\rho l$. C_V, C_D and C_L are the virtual mass coefficient, the drag coefficient, and the lift coefficient respectively.

Vorticity equation and orthogonal decomposition of liquid velocity

When taking the curl of Eq. (3), the vorticity equation for the bubbly flow is derived:

$$\frac{\partial \boldsymbol{\omega}}{\partial t} + \nabla \cdot (\boldsymbol{\omega}\boldsymbol{u}_l) = \nabla \cdot (\boldsymbol{u}_l \boldsymbol{\omega}) + \frac{\nu_l}{\alpha_l}\nabla^2 \boldsymbol{\omega} + \frac{1}{\alpha_l}\nabla \alpha_l \times \left(\boldsymbol{g} - \frac{\mathrm{D}\boldsymbol{u}_l}{\mathrm{D}t}\right) \tag{5}$$

where $\boldsymbol{\omega}$ is the vorticity of the liquid-phase.

$$\boldsymbol{\omega} = \nabla \times \boldsymbol{u}_l \tag{6}$$

According to the Helmholtz theorem, any vector field can be represented as the summation of the gradient of a scalar potential ϕ and the curl of a vector potential $\boldsymbol{\psi}$. The liquid velocity $\boldsymbol{u}_l$ is thus expressed as

$$\boldsymbol{u}_l = \nabla\phi + \nabla \times \boldsymbol{\psi} \tag{7}$$

The velocity calculated from Eq. (7) remains unaltered when any gradient of a scalar function is added to $\boldsymbol{\psi}$. To remove this arbitrariness, the following solenoidal condition is imposed on $\boldsymbol{\psi}$:

$$\nabla \cdot \boldsymbol{\psi} = 0 \tag{8}$$

When substituting Eq. (7) into Eq. (1), the following equation is obtained:

$$\frac{\partial \alpha_l}{\partial t} + \nabla \cdot \left[\alpha_l (\nabla\phi + \nabla \times \boldsymbol{\psi})\right] = 0 \tag{9}$$

Taking the curl of Eq. (7) and substituting Eq. (8) into the resultant equation, the following vector Poisson equation for $\boldsymbol{\psi}$ is derived:

$$\nabla^2 \boldsymbol{\psi} = -\boldsymbol{\omega} \tag{10}$$

Simulation Based on VIC Method

Discretization of vorticity field into vortex elements

Once ϕ and $\boldsymbol{\psi}$ have been computed from Eqs. (9) and (10) respectively, the velocity $\boldsymbol{u}_l$ is calculated from Eq. (7). The vorticity $\boldsymbol{\omega}$ in Eq. (10) is estimated from Eq. (5). The VIC method discretizes the vorticity field into vortex elements and calculates the distribution of $\boldsymbol{\omega}$ by tracing the convection of each vortex element.

It is postulated that the position vector and vorticity for the vortex element p are $\boldsymbol{x}_p=(x_p, y_p, z_p)$ and $\boldsymbol{\omega}_p$, respectively. The Lagrangian form of the vorticity equation, Eq. (5), is written as follows:

$$\frac{\mathrm{d}\boldsymbol{x}_p}{\mathrm{d}t} = \boldsymbol{u}_l \tag{11}$$

$$\frac{\mathrm{d}\boldsymbol{\omega}_p}{\mathrm{d}t} = \nabla \cdot (\boldsymbol{u}_l \boldsymbol{\omega}) + \frac{\nu_l}{\alpha_l}\nabla^2 \boldsymbol{\omega} + \frac{1}{\alpha_l}\nabla \alpha_l \times \left(\boldsymbol{g} - \frac{\mathrm{D}\boldsymbol{u}_l}{\mathrm{D}t}\right) \tag{12}$$

When the position and vorticity of a vortex element are known at time t, the values at $t+\Delta t$ are computed from Eqs. (11) and (12). In the VIC method, the flow field is divided into computational grid cells to define $\boldsymbol{\psi}$, ϕ and $\boldsymbol{\omega}$ on the grids. If $\boldsymbol{\omega}$ is defined at a position $\boldsymbol{x}_k=(x_k, y_k, z_k)$,

the vorticity $\boldsymbol{\omega}$ is assigned to $\boldsymbol{x}_k$, or a vortex element with vorticity $\boldsymbol{\omega}$ is redistributed onto $\boldsymbol{x}_k$.

$$\boldsymbol{\omega}(\boldsymbol{x}_k) = \sum_{p}^{N_v} \boldsymbol{\omega}_p W\left(\frac{x_k - x_p}{\Delta x}\right) W\left(\frac{y_k - y_p}{\Delta y}\right) W\left(\frac{z_k - z_p}{\Delta z}\right) \tag{13}$$

where N_v is the number of vortex elements, and Δx, Δy and Δz are the grid widths. For the redistribution function W, the following equation is employed [19].

$$W(\varepsilon) \begin{cases} 1 - 2.5\varepsilon^2 + 1.5|\varepsilon|^3 & |\varepsilon| < 1 \\ 0.5\left(2 - |\varepsilon|^2\right)\left(1 - |\varepsilon|\right) & 1 \le |\varepsilon| \le 2 \\ 0 & |\varepsilon| > 2 \end{cases} \tag{14}$$

Calculation of gas volume fraction

The abovementioned grid cells are also used to calculate the gas volume fraction α_g. The bubble diameter is prescribed to be smaller than the grid width on the basis of the assumption (a). When a bubble with volume v_r exists at a position $\boldsymbol{x}_g=(x_g, y_g, z_g)$, the α_g value at the grid point of $\boldsymbol{x}_q=(x_q, y_q, z_q)$ is calculated by the following equation:

$$\alpha_g(xq) = \sum_{r}^{N_b} \frac{v_r}{\Delta x \Delta y \Delta z} W_\alpha\left(\frac{x_q - x_g}{\Delta x}\right) W_\alpha\left(\frac{y_q - y_g}{\Delta y}\right) W_\alpha\left(\frac{z_q - z_g}{\Delta z}\right) \tag{15}$$

where N_b is the number of bubbles. For the function W_α, the following equation, which is the redistribution function of vortex element [19], is employed.

$$W_\alpha(\varepsilon) \begin{cases} 0.5\left(|\varepsilon| + 1.5\right)^2 - 1.5\left(|\varepsilon| + 0.5\right)^2 & |\varepsilon| \le 0.5 \\ 0.5\left(-|\varepsilon| + 1.5\right)^2 & 0.5 \le |\varepsilon| \le 0.5 \\ 0 & |\varepsilon| > 1.5 \end{cases} \tag{16}$$

Discretization with staggered grid and correction of vorticity

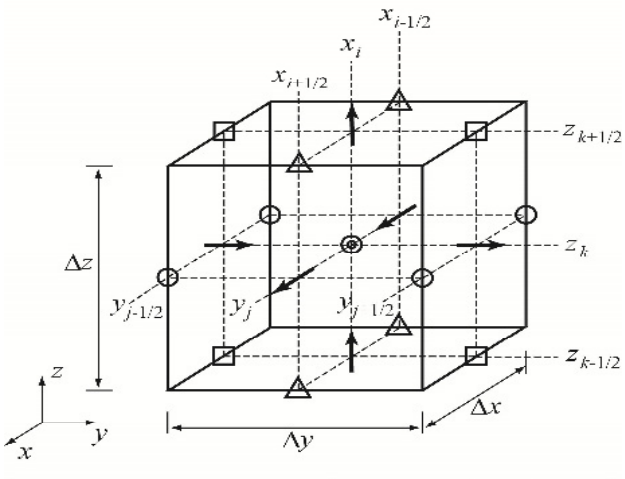

Figure 1: Computational grid and computed variables.

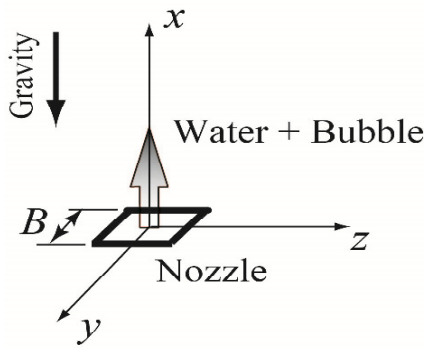

Figure 2: Square nozzle and coordinate system.

This simulation employs a staggered grid to solve Eqs. (9) and (10) so as to ensure consistency between the discretized equations and to prevent numerical oscillations of the solution. Figure 1 shows the grid. The scalar potential ϕ and the gas volume fraction α_g are defined at the center of a grid cell. The liquid velocity $\boldsymbol{u}_l$ is defined at the sides, while the vorticity $\boldsymbol{\omega}$ and the vector potential $\boldsymbol{\psi}$ are defined on the edges.

The vorticity field is discretized with vortex elements, and it is expressed by the superposition of the vorticity distribution around each vortex element as found from Eq. (13). Thus, the vorticity field obtained from Eq. (13), denoted by $\overline{\boldsymbol{\omega}}_r$, does not always satisfy the solenoidal condition. The curl of the velocity calculated by using $\overline{\boldsymbol{\omega}}_r$ results in the vorticity satisfying the solenoidal condition. This correction method for the vorticity is used in this simulation.

Numerical procedure

Given the flow at time t, the flow at $t+\Delta t$ is simulated by the following procedure:

1. Calculate the bubble motion from Eq. (4).
2. Calculate α_g from Eq. (15), and compute α_l from Eq. (2).
3. Calculate the time variation of ω at every grid point from Eq. (12).
4. Calculate the convection of each vortex element from Eq. (11).
5. Calculate ω from Eq. (13).
6. Calculate ψ from Eq. (10).
7. Calculate ϕ from Eq. (9).
8. Calculate $\boldsymbol{u}_l$ from Eq. (7).
9. Correct the vorticity, or calculate the corrected vorticity from the curl of $\boldsymbol{u}_l$.

Simulation Conditions

A bubbly jet issuing from a nozzle having a square cross-section is simulated. The flow direction is vertically upward. The nozzle and the coordinate system are shown in Figure 2. The y-z plane is horizontal, and the x-axis is taken in the vertically upward direction along the jet centerline.

Table 1 lists the simulation conditions, Air-water bubbly mixtures issues from the nozzle. The side length of the nozzle exit B is 10 mm. The computational domain consists of a hexahedral region of 45B×30B×30B. It is divided into 150×300×300 grid cells. A simulation using more computational cells 180×360×360 was preliminarily performed. But

Two-phase mixtures	Air/Water
Side length of nozzle cross-section; B	10 mm
Computational domain	$45B\times30B\times30B$
Number of grids	150×300×300
Reynolds number; $U_0 B/\nu_l$	5000
Bubble diameter; d	0.2 mm
Bubble volumetric flow rate ratio	0.0025
Lift coefficient; C_L	0.5
Virtual mass coefficient; C_V	0.5
Time increment; $U_0 \Delta t/B$	0.015

Table 1: Simulation conditions.

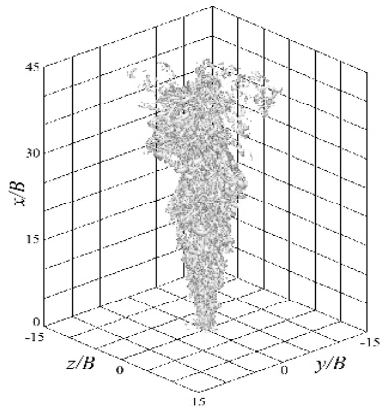

Figure 3: Iso-surface of Q value for single-phase jet ($Q/(U_0/B)^2=0.01$).

the bubble distribution and the water velocity field were less affected by the increase in the number of cells. Therefore, the cell size is found to be appropriate. The water has a uniform velocity U_0 at the nozzle exit, and the Reynolds number Re ($=U_0B/\nu_l$) is 5000. The time increment Δt is set at $U_0\Delta t/B=0.015$.

The bubble diameter d is 0.2 mm. The bubble volumetric flow rate ratio at the nozzle exit is 0.0025. The bubbles are released from the nozzle exit at a time interval Δt with the same velocity as the water. The number of released bubbles is specified by the volumetric flow rate ratio. The releasing positions are determined by using random numbers. The relation of $C_L=C_V=0.5$ is used in Eq. (4) [18], and the drag coefficient C_D is given as:

$$C_D=\max\left\{\frac{48}{\mathrm{Re}_b}\left(1-\frac{2.21}{\mathrm{Re}_b^{1/2}}\right),\frac{24}{\mathrm{Re}_b}\right\} \quad (17)$$

where Re_b is the bubble Reynolds number defined as $d\left|\boldsymbol{u}_g-\boldsymbol{u}_l\right|/\nu_l$. Equation (17) combines the theoretical formula of Moore [20] and the Stokesian drag coefficient. It was also used for a bubble plume simulation by Murai and Matsumoto [21].

A non-slip condition is imposed on the boundary ($x/B=0$), on which the nozzle exit is mounted. The velocity gradient is set at zero on the other boundaries [22]. The Poisson equations, Eqs. (9) and (10), are solved by the SOR method.

Results and Discussions

Single-phase water jet

First, the present method is applied to simulate the single-phase water jet. When the developed jet occurs, the iso-surface for the second invariant of the velocity gradient tensor Q distributes as shown in Figure 3. The vortical structure, in which vortex tubes having various scales entangle, is grasped.

Figure 4 shows the vorticity component parallel to the jet axis at the same time point as Figure 3, where the iso-surfaces of $\omega_x/(U_0/B)=\pm$ 0.002 are plotted. Pairs of positive and negative vortex tubes exist and entangle, suggesting the appearance of highly three-dimensional vertical flow.

The mean velocity on the jet centerline u_k changes as a function of the axial distance from the nozzle as shown in Figure 5. The velocity decays markedly at $x/B \geq 2$. Mi et al. [23] measured the velocity distribution of a jet of Re=15000 at the fully-developed region. The present result agrees nearly with the measurement. The velocity decay at the fully-developed region of the jet satisfies a relation of $u_{lc} \propto x^{-1}$

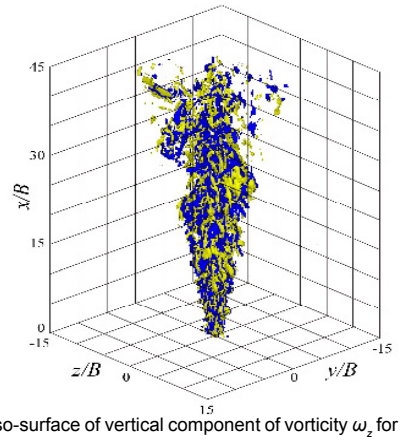

Figure 4: Iso-surface of vertical component of vorticity ω_z for single-phase jet ($\omega_z/(U_0/B)=\pm$ 0.002).

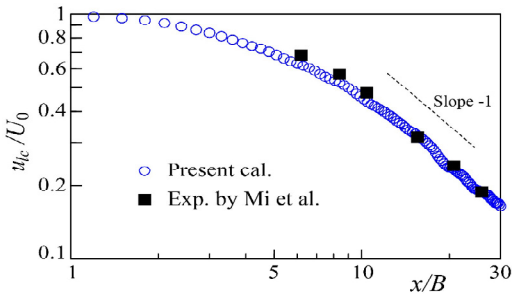

Figure 5: Axial evolution of centerline velocity for single-phase jet.

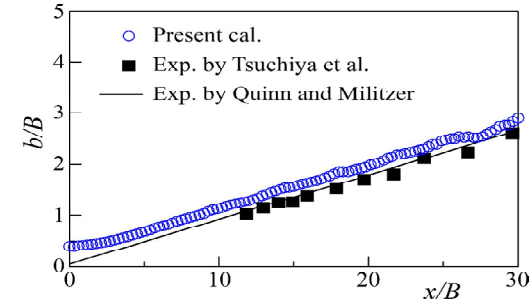

Figure 6: Axial evolution of half-width for single-phase jet.

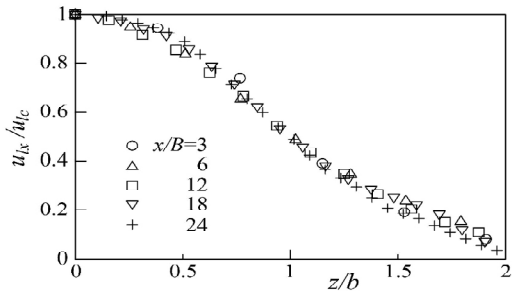

Figure 7: Lateral distribution of velocity for single-phase jet.

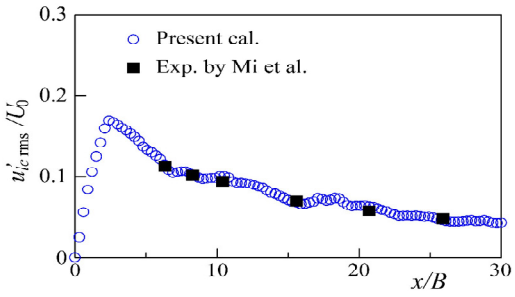

Figure 8: Axial evolution of axial turbulence intensity on centerline for single-phase jet.

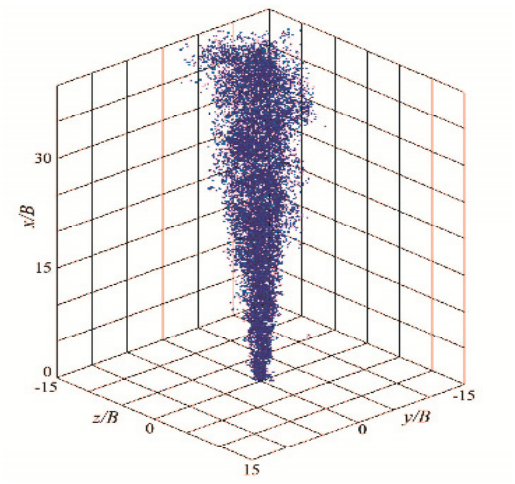

Figure 9: Bubble distribution in fully developed bubbly.

[24]. In this simulation, such relation is obtained.

The change in the half-width b is shown in Figure 6. The present result is slightly larger than the measured one by Tsuchiya et al. [25] and the experimental formula of Quinn and Militzer [26]. The change in the axial direction is favorably computed.

Figure 7 shows the lateral distribution of the time-averaged axial velocity u_{lx}, where the centerline velocity u_{lc} and the half-width b are used for the nondimensional expression. Though the effect of the potential core appears on the section at x/B=3, the similarity of velocity distribution is analyzed on the sections at $x/B \geq 6$.

The axial component of the turbulent intensity u'_{lcrms} on the jet centerline varies as shown in Figure 8. It takes the maximum value at x/B=2.4. The present result agrees well with the measured one of Mi et al. [23] at the fully-developed region.

From the abovementioned results, one can confirm the validity of the present method for single-phase jet simulations.

Bubble distribution and vortical structure

Figure 9 shows the bubble distribution of the fully-developed bubbly jet. The bubbles disperse markedly in the lateral (horizontal) direction at $x/B \geq 4.3$. This is attributable to the water momentum diffusion in the direction. The dispersion becomes larger with increasing axial distance from the nozzle.

According to Clift et al. [27], the shape of a bubble rising in a viscous fluid under the influence of gravity is specified by the bubble Reynolds number, $\mathrm{Re}_b = d\left|\boldsymbol{u}_g - \boldsymbol{u}_l\right|/\nu_l$, and the Eötvös number, $\mathrm{Eo} = g\left(\rho_l - \rho_g\right)d^2/\sigma$, where σ is the surface tension. In this simulation, Re_b is less than 16.1 and Eo=0.0527. The bubble shape is specified to be spherical [27], demonstrating the validity of the assumption (d).

The iso-surface of Q for the bubbly jet at the same time point as Figure 9 is presented in Figure 10. When compared with the result for the single-phase water jet shown in Figure 3, the vortical region spreads more in the horizontal direction at $x/B \leq 7$. One can grasp the increase in the jet width due to the bubbles. But the width of the vortical region reduces at $x/B \geq 30$. The bubbles hardly affect the scale of the vortex tubes.

Figure 11 shows the iso-surfaces of the axial component of the vorticity at the same time point as Figure 10. The iso-surfaces are divided into finer ones when compared with the result for the single-phase water jet (Figure 4). The three-dimensional features of the vortical structure become remarkable owing to the bubbles distributing non-uniformly in the jet.

Bubble motion and water velocity field

The mean velocities of water and bubble on the jet centerline change as function of the axial distance from the nozzle as shown in Figure 12. The water velocity of the bubbly jet is slightly lower than that of the single-phase jet at $x/B \leq 9.6$ while it is higher downstream of the

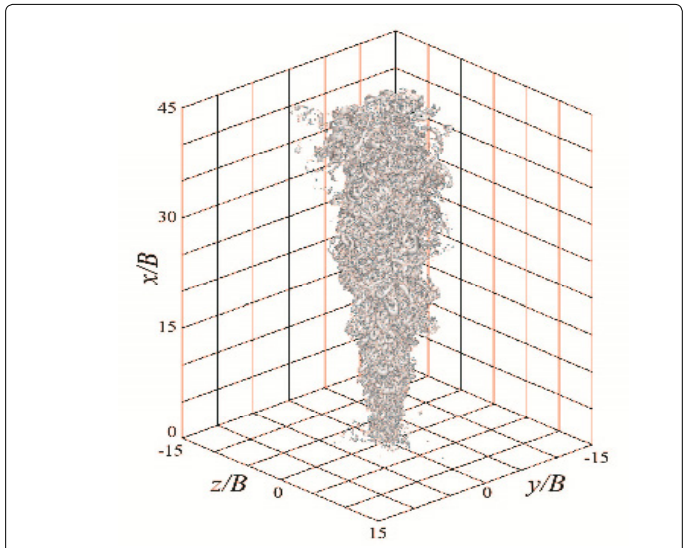

Figure 10: Iso-surface of Q value for bubbly jet ($Q/(U_l/B)^2$=0.01)).

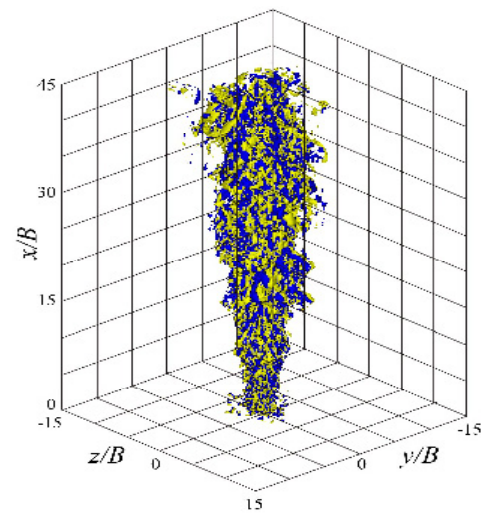

Figure 11: Iso-surface of vertical component of vorticity ω_z for bubbly jet ($\omega_z /(U_l/B)$=± 0.002).

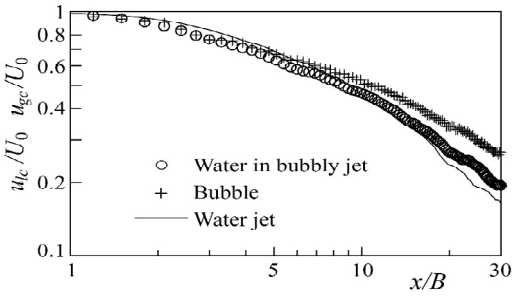

Figure 12: Axial evolution of centerline velocity for bubbly jet.

region. The bubble velocity is slightly higher than the water, because the buoyant force acts on them. The lesson of the water velocity of the bubbly jet at $x/B \leq 9.6$ is caused by the increase in the water momentum diffusion in the horizontal direction due to the bubbles as explained later. The relaxation of the water velocity decay at x/B>9.6 is attributable to the fact that the water is accelerated by the bubbles flowing faster than the water. The increase in the water momentum diffusion due to the bubbles at jet initial region was also clarified experimentally by Kumar et al. [12].

A numerical simulation of an air jet laden with small solid particles (diameter 100 μm, density 2590 kg/m^3) also made clear such air velocity reduction at the jet initial region [28]. It seems that a dispersed phase has the similar disturbances on the continuous phase in jet flows.

Figure 13 shows the axial evolution of the half-width of the water velocity. At $x/B \leq 7.5$, the half-width of the bubbly jet is larger than that of the single-phase jet. This is caused by the abovementioned increase in the water momentum diffusion in the lateral direction due to the bubbles. At $x/B \geq 7.5$, it is smaller because the velocity decay is relaxed as shown in Figure 12.

The lateral distribution of the water and bubble velocities is presented in Figure 14, where the water velocity at the nozzle exit U_0 and the half-width for the single-phase jet b are used for the non-dimensional expression. On the sections at x/B=3 and 12, the bubble velocity is higher than the water. On the section at x/B=3, the water velocity of the bubbly jet is slightly lower and higher than the single-phase jet at $z/b \leq 0.86$ and $z/B \geq 0.86$, respectively. This is because the water momentum diffusion in the lateral direction increases due to the bubbles. On the section at x/B=1, the water velocity of the bubbly jet is higher than the single-phase jet. This is attributable to the acceleration effect by the bubbles. The velocity difference caused by the bubbles is lower than that on the section at x/B=3.

The axial component of the water turbulence intensity distributes on the jet centerline as shown in Figure 15. The turbulence intensity of the bubbly jet is larger than that of the single-phase jet. This result is parallel with the measured one of Kumar [12].

Figure 16 shows the lateral distribution of the axial component of the water turbulence intensity. The intensity is heightened by the bubbles. The marked increase is observed on the section at x/B=3, where the water momentum diffusion is promoted by the bubbles.

In Figures 14, 15 and 16, it is found that the bubble effects on the water flow lessen with increasing axial distance from the nozzle. This is because the bubbles disperse in the lateral (horizontal) direction, and accordingly the bubble volume fraction around the jet centerline reduces. Such decrease in the bubble effect was also reported by Kumar [12].

Conclusions

An air-water bubbly jet, issuing vertically upward from a nozzle of a square-cross section, is simulated. The Vortex in Cell method for

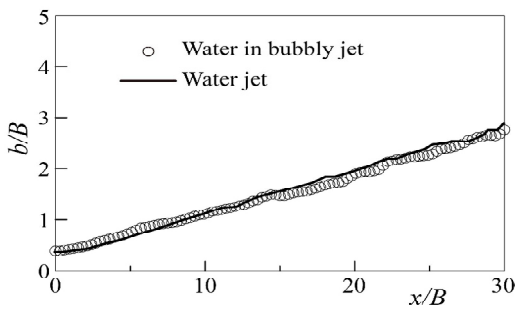

Figure 13: Axial evolution of half-width for bubbly jet.

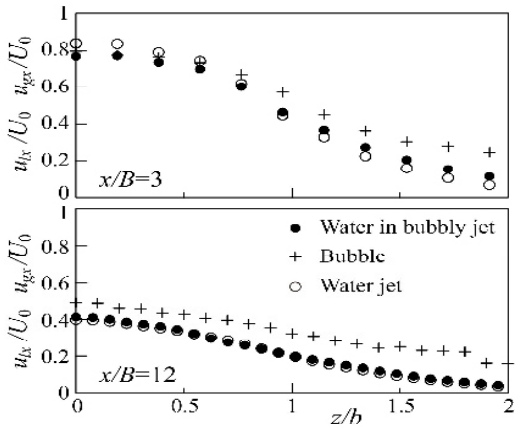

Figure 14: Lateral distribution of velocity for bubbly jet.

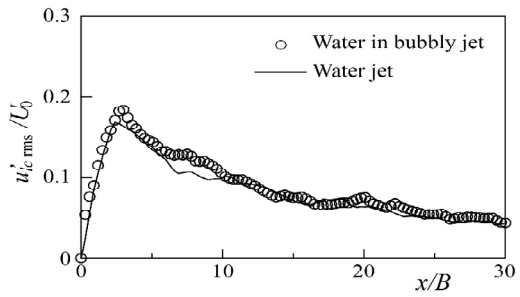

Figure 15: Axial evolution of axial turbulence intensity of water on centerline in bubbly jet.

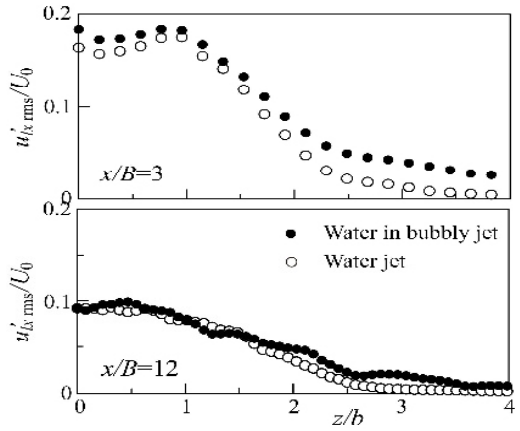

Figure 16: Lateral distribution of axial turbulence intensity of water in bubbly jet.

bubbly flow proposed by the authors in a prior study is used for the simulation. The Reynolds number of the water is 5000, the bubble diameter is 0.2 mm, and the bubble volumetric flow rate ratio at the nozzle exit is 0.0025. The results are summarized as follows:

(1) The bubbles heighten the water turbulence intensity and cause the increase in the water momentum diffusion in the lateral direction at the initial region of the jet. This simulated result is in good agreement with the existing measured one, demonstrating the validity of the simulation method.

(2) At the developed region, the water velocity decay is relaxed and the spread of the jet in the lateral direction decreases. This is because the bubbles have the higher velocity than the water.

(3) The three-dimensional features of the water vortical structure become more remarkable owing to the bubbles.

References

1. Christiansen IP (1973) Numerical simulation of hydrodynamics by the method of point Vortices. J Comput Phys 13: 363-379.
2. Cottet GH, Poncet P (2003) Advances in direct numerical simulations of 3D wall-bounded flows by Vortex-in-Cell methods. J Comput Phys 193: 136-158.
3. Cocle R, Winckelmans G, Daeninck G (2008) Combining the vortex-in-cell and parallel fast multipole methods for efficient domain decomposition simulations. J Comput Phys 227: 9091-9120.
4. Chatelain P, Curioni A, Bergdorf M, Rossinelli D, Andreoni W, et al. (2008) Billion vortex particle direct numerical simulations of aircraft wakes. Comput Methods in Appl Mech Eng 197: 1296-1304.
5. Uchiyama T, Yoshii Y, Hamada H (2014) Direct numerical simulation of a turbulent channel flow by an improved vortex in cell method. Int J Numerical Methods for Heat and Fluid Flow 24: 103-123.
6. Uchiyama T, (2012) Numerical simulation of interaction between a vortex ring and gas bubbles. Fortschritt-Berichte VDI, Reihe 929: 36-50.
7. Uchiyama T (2013) Numerical simulation of particle-laden gas flow by vortex in cell method. Powder Technology 235: 376-385.
8. Uchiyama T, Shimada S (2014) Numerical simulation of the interactions between a vortex pair and solid particles near a wall. Powder Technology 257: 55-67.
9. Milenkovic RZ, Sigg B, Yadigaroglu G (2007) Bubble clustering and trapping in large vortices. Part 1: Triggered bubbly jets investigated by phase-averaging. Int J Multiphase Flow 33: 1088-1110.
10. Sun TY, Faeth GM (1986) Structure of turbulent bubbly jets-I. methods and centerline properties. Int J Multiphase Flow 12: 99-114.
11. Sun TY, Faeth GM (1986) Structure of turbulent bubbly jets-II. phase property profiles. Int J Multiphase Flow 12: 115-126.
12. Kumar S, Nikitopoulos DN, Michaelides EE (1989) Effect of bubbles on the turbulence near the exit of a liquid jet. Exp Fluids 7: 487-494.
13. Iguchi M, Okita K, Nakatani T, Kasai N (1997) Structure of turbulent round bubbling jet generated by premixed gas and liquid injection. Int J Multiphase Flow 23: 249-262.
14. Lima Neto IE, Zhu DZ, Rajaratnam N (2008) Bubbly jets in stagnant water. Int J Multiphase Flow 34: 1130-1141.
15. Shuen JS, Chen L-D, Faeth GM (1983) Evaluation of a stochastic model of particle dispersion in a turbulent round jet. AIChE J 29: 167-170.
16. Xing T, Li Z, Frankel SH (2005) Numerical simulation of vortex cavitation in a three-dimensional submerged transitional jet. Trans ASME J Fluid Eng 127: 714-725.
17. Auton TR, Hunt JCR, Prud'homme M (1988) The force exerted on a body in inviscid unsteady non-uniform rotational flow. J Fluid Mech 197: 241-257.
18. Yang X, Thomas NH, Guo LJ, Hou Y (2002) Two-way coupled bubble laden mixing Layer. Chem Eng Sci 57: 555-564.
19. Cottet GH, Koumoutsakos P (2000) Vortex Methods: Theory and Applications. Cambridge Univ Press, Cambridge.
20. Moore DW (1963) The boundary layer on a spherical gas bubble. J Fluid Mech 16: 161-176.
21. Murai Y, Matsumoto Y (1997) Numerical analysis of detailed flow structures in bubble plume. 2nd Report, three-dimensional flow structure and turbulence mechanism. JSME Int J Ser B 63: 2283-2288.
22. Gresho PM (1991) Some current CFD issues relevant to the incompressible Navier-Stokes equations. Comput Methods Appl Mech Engg 87: 201-252.
23. Mi J, Nathan GJ, Luxton RE (2000) Centerline mixing characteristics of jets from nine differently shaped nozzles. Exp Fluids 28: 93-94.
24. Sforza PM, Steiger MH, Trentacoste N (1966) Studies on three-dimensional viscous Jets. AIAA J 4: 800-806.
25. Tsuchiya Y, Horikoshi C, Sato T (1986) On the spread of rectangular jets. Exp Fluids 4: 107-204.
26. Quinn WR, Militzer J (1988) Experimental and numerical study of a turbulent free square jet. Phys Fluids 31: 1017-1025.
27. Clift R, Grace JR, Weber ME (1978) Bubbles, Drops, and Particles. Academic Press, New York.
28. Uchiyama T, Fukase A (2005) Three-dimensional vortex method for gas-particle two-phase compound round jet. Trans ASME J Fluid Eng 127: 32-40.